Intravital quantification of absolute cytoplasmic B cell calcium reveals dynamic signaling across B cell differentiation stages

Carolin Ulbricht[1,2], Ruth Leben[2], Asylkhan Rakhymzhan[2], Frank Kirchhoff[3], Lars Nitschke[4], Helena Radbruch[1], Raluca A Niesner[5,2*], Anja E Hauser[1,2*]

[1]Charité - Universitätsmedizin Berlin
[2]Deutsches Rheuma-Forschungszentrum Berlin, ein Institut der Leibniz-Gemeinschaft
[3]Universität des Saarlandes, Homburg
[4]Friedrich-Alexander-Universität Erlangen-Nürnberg
[5]Freie Universität Berlin

*equal contribution

Correspondence to: Anja Hauser, anja.hauser-hankeln@charite.de, hauser@drfz.de

Abstract

Development, function and maintenance of lymphocytes largely depend upon the cellular mobilization and storage of Ca^{2+} ions. In B lymphocytes, the absolute amount of calcium mobilized and retained after cell signaling remains unknown, athough it is a crucial part of their selection within germinal centers and differentiation into plasma cells. Here, we introduce the novel reporter mouse strain YellowCaB that expresses the genetically encoded calcium indicator TN-XXL in $CD19^{+}$ lymphocytes. The construct consists of the electron-donor fluorophore eCFP and the acceptor citrine, linked by a calcium sensitive domain. Its conformation and therefore donor quenching is directly linked to cytosolic calcium concentrations. By combining intravital two-photon fluorescence lifetime microscopy with our numerical approach for phasor-based analysis, we are able to extract absolute cytoplasmic calcium concentrations in activated B cells for the first time *in vivo*. We show that calcium concentrations in B cells are highly dynamic and fluctuations persist in extrafollicular B cells with functional relevance.

Introduction

The capacity of the immune system to produce a variety of different antibodies and to further fine-tune their affinity to bind antigen (AG) upon pathogen challenge is one of the pillars of adaptive humoral immunity. Fine-tuning is achieved by somatic hypermutation of immunoglobulin genes, followed by a T cell-aided selection process, which B cells undergo within germinal centers (GC). This eventually results in a pool of high affinity memory B cells and long-lived plasma cells[1–3]. B cells encounter and take up membrane-bound AG in the form of immune complexes on follicular dendritic cells (FDCs) in GCs. This leads to B cell receptor (BCR) activation and calcium influx into the cell[4]. This eventually switches on

effector proteins and transcription factors like nuclear factor kappa B (NF-κB), nuclear factor of activated T cells (NFAT), or Myelocytomatosis oncogene cellular homolog (c-Myc), thereby activating the B cells, inducing differentiation events and remodeling of metabolic requirements [5–10]. BCR-affinity dependent AG-capture has been thought to serve solemnly the processing and MHCII-dependent presentation to follicular helper T cells and that signaling is dampened[11]. However, newer studies show that BCR activated calcium signaling has to precede T cell derived signals and that the latter have to occur within a limited period of time after initial BCR activation[12]. Changes in cytoplasmic calcium concentration thus could provide a mechanistic link between BCR signal strength, the switch-on of downstream effector processes and their temporal regulation.

In contrast to qualitative description, absolute quantification of cytosolic calcium has not been achieved yet, partly because of the lack of internal concentration standards. Two-fluorophore Förster resonance energy transfer (FRET)-GECI, that can take on a calcium-saturated (quenched) and calcium-unsaturated (unquenched) condition, could overcome this, however, its intravital application has been hampered by light distortion effects in deeper tissue. The differential scattering and photobleaching properties of the two fluorophores would lead to a false bias towards a higher quenching state. We here introduce a single-cell fluorescence lifetime imaging (FLIM) approach for absolute calcium quantification in living organisms that is tissue depth-independent. The eCFP/citrine-FRET pair-GECI TN-XXL is able to measure fluctuations in cytoplasmic calcium concentration through the calcium binding property of the muscle protein Troponin C (TnC)[13]. Calcium binding to the fluorophore-linker TnC quenches eCFP fluorescence through energy scavenging by citrine, linking decreasing eCFP fluorescence lifetime to increasing calcium concentration. In addition, phasor analysis of FLIM data elegantly condenses multicomponent fluorescent decay curves into single vector-based information (the phasor)[14]. For calcium concentration analysis in microscopic images, we took advantage of this by projecting the phasor value in each pixel onto a given calibration[15]. With this method, we are able to describe short- and long-term changes in absolute calcium concentrations within B cells during affinity maturation and differentiation into antibody-producing plasma cells.

We here show, using our calcium reporter mouse strain “YellowCaB” (<u>yellow</u> fluorescence after <u>ca</u>lcium influx in <u>B</u> cells), which expresses cytosolic TN-XXL under control of the CD19 promoter, that calcium signals are highly dynamic within different B cell populations. We analyze AG-specific and non-AG-specific extrafollicular and GC B cells as well as AG-specific extrafollicular plasma blasts. We describe highly dynamic signaling patterns that differ in amplitude and baseline and correlate with cellular differentiation stages.

Results

73 **YellowCaB: A system for FRET-based calcium analysis in B cells**

74 By breeding mice expressing a loxP-flanked STOP sequence followed by the TN-XXL-
75 construct inserted into the ROSA26 locus together with the CD19-Cre strain[16], we generated
76 offspring with exclusive and visible expression of the FRET fluorophore pair eCFP and citrine
77 in $CD19^{+}$ B lymphocytes, as confirmed by confocal microscopy after magnetic B cell isolation
78 (Fig 1a and b). YellowCaB cells were excited with a 405nm Laser that is capable of exciting
79 eCFP but not citrine. The detection of yellow emission thus can be attributed to baseline
80 FRET representing steady state calcium levels. Expression of TN-XXL in YellowCaB mice
81 was tested by flow cytometry, determining the percentage of fluorescent cells in a
82 $CD19^{+}GFP^{+}$ gate after excitation with the 488nm laser. Yellow citrine fluorescence was found
83 to be exclusive to $CD19^{+}$ B lymphocytes and the expression level of TN-XXL ranged between
84 25-45% in mice expressing the sensor on one allele ($CD19^{cre/+}$ TN-$XXL^{+/-}$) and 70-90% in
85 mice homozygous for the TN-XXL construct ($CD19^{cre/+}$ TN-$XXL^{+/+}$) animals (Fig 1c and S1).
86 When analyzing secondary lymphoid organs, no differences in total cell numbers and B cell
87 numbers between TN-$XXL^{+/-}$ $CD19^{cre/+}$, TN-$XXL^{+/+}$ $CD19^{cre/+}$ and wild type mice were detected
88 (Fig S1). We next set out to test if we could induce a FRET signal change under calcium-
89 saturating conditions in the cytoplasm. The ionophore ionomycin is commonly used as
90 positive control in *in vitro* experiments measuring calcium concentrations, as it uncouples the
91 increase of calcium concentration from the physiological entry sites of Ca^{2+} ions by forming
92 holes in the cell membrane. When stimulated with ionomycin, a steep increase of the FRET
93 level over baseline could be recorded by flow cytometry in the GFP-channel after excitation
94 with the 405nm laser. Calcium-dependence was independently confirmed by staining with
95 the calcium sensitive dye X-Rhod-1 that shows a red fluorescence signal increase after
96 calcium binding (Fig 1d)[17].

97 In preparation of our intravital imaging experiments, we first needed to test if the YellowCaB
98 system is stable enough for time-resolved microscopic measurements and sensitive enough
99 for subtle cytoplasmic calcium concentration changes as they occur after store-operated
100 calcium entry (SOCE). In SOCE, stimulation of the BCR with AG leads to drainage of
101 intracellular calcium stores in the endoplasmic reticulum (ER) which triggers calcium influx
102 from the extracellular space into the cytosol through specialized channels[18]. We established
103 a customizable continuous perfusion flow chamber image system to monitor and manipulate
104 YellowCaB cells over the duration of minutes to hours (Fig. 1e). Division of the fluorescence
105 intensity of electron acceptor citrine by that of donor eCFP yields the FRET ratio (R), which is
106 then put into relationship to baseline FRET levels. As citrine intensity is expected to increase
107 and eCFP intensity is expected to decrease due to FRET, the resulting value of $\Delta R/R$ will
108 increase as well. As expected, we could detect a decrease of the CFP signal, concurrent with

109 an increased YFP fluorescence after the addition of 4µg/ml ionomycin to continuous flow of
110 6mM Krebs-Ringer solution. Overall, this resulted in a maximal elevation of ΔR/R of 50-55%
111 over baseline (Fig. 1f). Analysis of >100 cells showed that approximately in three quarters of
112 the cells we were able to detect FRET in response to ionomycin treatment, and that the
113 majority of these cells showed 35-40% FRET signal change. According to the two
114 populations visible in the histogram, we defined a change of 20% ΔR/R as a relevant
115 threshold for the positive evaluation of responsiveness (Fig. 1g). In conclusion, we achieve
116 the functional and well tolerated expression of TN-XXL exclusively in murine $CD19^+$ B cells
117 for measurement of changes of cytoplasmic calcium concentrations. Moreover, flow
118 cytometric and microscopic long-term calcium analysis are possible.

119

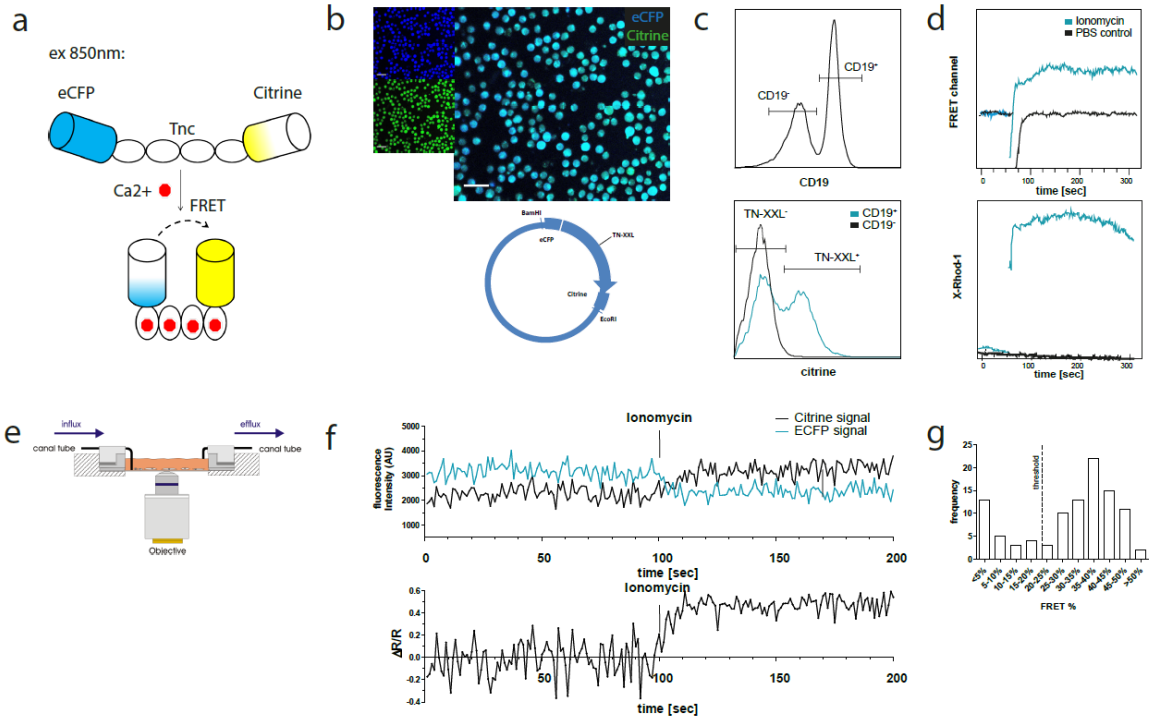

120

121 Fig. 1 The GECI TN-XXL is functionally expressed in $CD19^+$ B cells of YellowCaB mice. a Schematic representation of the
122 genetically encoded calcium indicator TN-XXL with calcium sensitive domain TnC fused to donor fluorophore eCFP and
123 acceptor fluorophore citrine. Binding of Ca^{2+} ions within (up to) four loops of TnC leads to quenching of eCFP and Förster
124 resonance energy transfer to citrine. b Confocal image of freshly isolated $CD19^+$ B cells. Overlapping blue and yellow-green
125 fluorescence of eCFP and citrine, respectively, can be detected after cre-loxP mediated expression of the TN-XXL vector in
126 YellowCaB mice. c Flow cytometric analysis of TN-XXL expression among lymphocytes of YellowCaB mice. d Flow cytometric
127 measurement of calcium flux after addition of ionomycin and PBS control. e Continuous perfusion imaging chamber for live
128 cell imaging. f Confocal measurement of mean fluorescence intensity and FRET signal change after addition of ionomycin to
129 continuous perfused YellowCaB cells. Data representative for at least 100 cells out of three independent experiments. g
130 Frequency histogram of >100 YellowCaB single cells, FRET analyzed after ionomycin stimulation. Threshold chosen for
131 positive FRET signal change = 20% over baseline intensity.

132 **Repeated BCR stimulation results in fluctuating cytoplasmic calcium concentrations**

133 SOCE in B cells can be provoked experimentally by stimulation of the BCR with multivalent

134 AG, for example anti-Ig heavy chain $F(ab)_2$ fragments. To test the functional performance of
135 the GECI TN-XXL in YellowCaB cells, we stimulated isolated YellowCaB cells with 10 µg/ml
136 anti-IgM $F(ab)_2$ fragments to activate the BCR. In an open culture imaging chamber, we
137 could induce an elevated FRET signal with a peak height of >30% that lasted over three
138 minutes (Fig 2a). The signal declines after this time span, probably due to BCR
139 internalization or the activity of ion pumps. We tested antibody concentrations at 2 µg/ml,
140 4 µg/ml, 10 µg/ml and 20 µg/ml. An antibody concentration of 2 µg/ml was not enough to
141 provoke calcium flux (data not shown), whereas at 4 µg/ml anti-IgM-$F(ab)_2$ we could observe
142 20% elevated ΔR/R over baseline (Fig. 2b). At 20 µg/ml anti-IgM-$F(ab)_2$ we could see no
143 further FRET increase (Fig S2). Thus, we conclude a concentration dependency of the GECI
144 TN-XXL and saturating conditions at 10 µg/ml BCR heavy chain stimulation. Interestingly,
145 the reaction is not completely cut off after the FRET signal has declined, but a residual FRET
146 signal of about 7% compared to baseline values can be measured for approximately 3.5
147 additional minutes (Fig. 2a). Thus, B cells seem to be able to store extra calcium within the
148 cytoplasm for some time. We therefore asked if it is possible to stimulate YellowCaB cells
149 more than once. Indeed, we could stimulate YellowCaB cells *in vitro* repeatedly with $F(ab)_2$-
150 fragments of anti-IgM-antibody. For this purpose, we connected our imaging culture chamber
151 to a peristaltic pump and took advantage of the fact that under continuous perfusion with
152 Ringer solution, the flow will dilute the antibody out of the chamber. This way, it is possible to
153 stimulate B cells several times rapidly and subsequently, before BCRs are internalized (Fig.
154 2b), indicated by multiple peaks in ΔR/R. We repeated this procedure several times and
155 could observe this type of repetitive response up to five times. Also, stimulation of the BCR
156 light chain using an anti-kappa antibody leads to calcium increase within YellowCaB cells
157 (Fig. S2). Of note, the resulting FRET peak is shaped differently, and concentrations
158 >150µg/ml antibody were needed in order to generate a response. This might be in part due
159 to the fact that monovalent AG is not sufficient to drive BCR activation and the light chain has
160 different conformational properties.

161 Since T cell engagement and the binding of unspecific microbial targets to innate receptors
162 like Toll like receptors (TLRs) have also been described to raise cytoplasmic calcium in B
163 cells[19–21], we investigated the response of YellowCaB cells after incubation with anti-CD40
164 antibodies, as well as the TLR4 and TLR9 stimuli Lipopolysaccharide and cytosine-
165 phosphate-guanin-rich regions of bacterial DNA (CpG), respectively. Within the same cells,
166 we could detect no reaction to anti-CD40 treatment alone, but observed three types of
167 shapes in post-CD40 BCR-stimulated calcium responses, that differed from anti-CD40-
168 untreated cells (Fig. 2a). These calcium flux patterns were either sustained, transient or of an
169 intermediate shape (Fig. 2c). Sustained calcium flux even saturated the sensor at a level
170 comparable to that achieved by ionomycin treatment. Cells that showed only intermediate

171 flux maintained their ability to respond to ionomycin treatment at high FRET levels, as
172 demonstrated by the ΔR/R reaching 0.4 again after stimulation (Fig. 2c). Furthermore,
173 integrated TLR and BCR stimulation affected the appearance of the calcium signal. The
174 addition of TLR9 stimulus CpG alone had no effect on YellowCaB FRET levels, however, the
175 subsequent FRET peak in response to anti-Ig-F(ab)$_2$ was delayed (Fig 2d+e). TLR4
176 stimulation via LPS could elevate calcium concentration of B cells, but only to a minor extent
177 (Fig 2e). Pre-BCR TLR4 stimulation by LPS lead to decreased FRET levels in response to
178 anti-IgM-F(ab)$_2$. We conclude that, in order to get fully activated, B cells are able to collect
179 and integrate multiple BCR-induced calcium signals and that signaling patterns are further
180 shaped by innate signals or T cell help. BCR-inhibition abolishes a FRET signal change in
181 response to anti-IgM-F(ab)$_2$ (Fig S2). Of note, we excluded the possibility that measured
182 signal changes were related to chemokine stimulation. *In vitro*, we could detect no FRET
183 peak after applying CXCL12, probably because of lacking GECI sensitivity to small
184 cytoplasmic changes (Fig. S2). Thus, the YellowCaB system is well suited for the detection
185 of BCR-induced cytosolic calcium concentration changes.

186

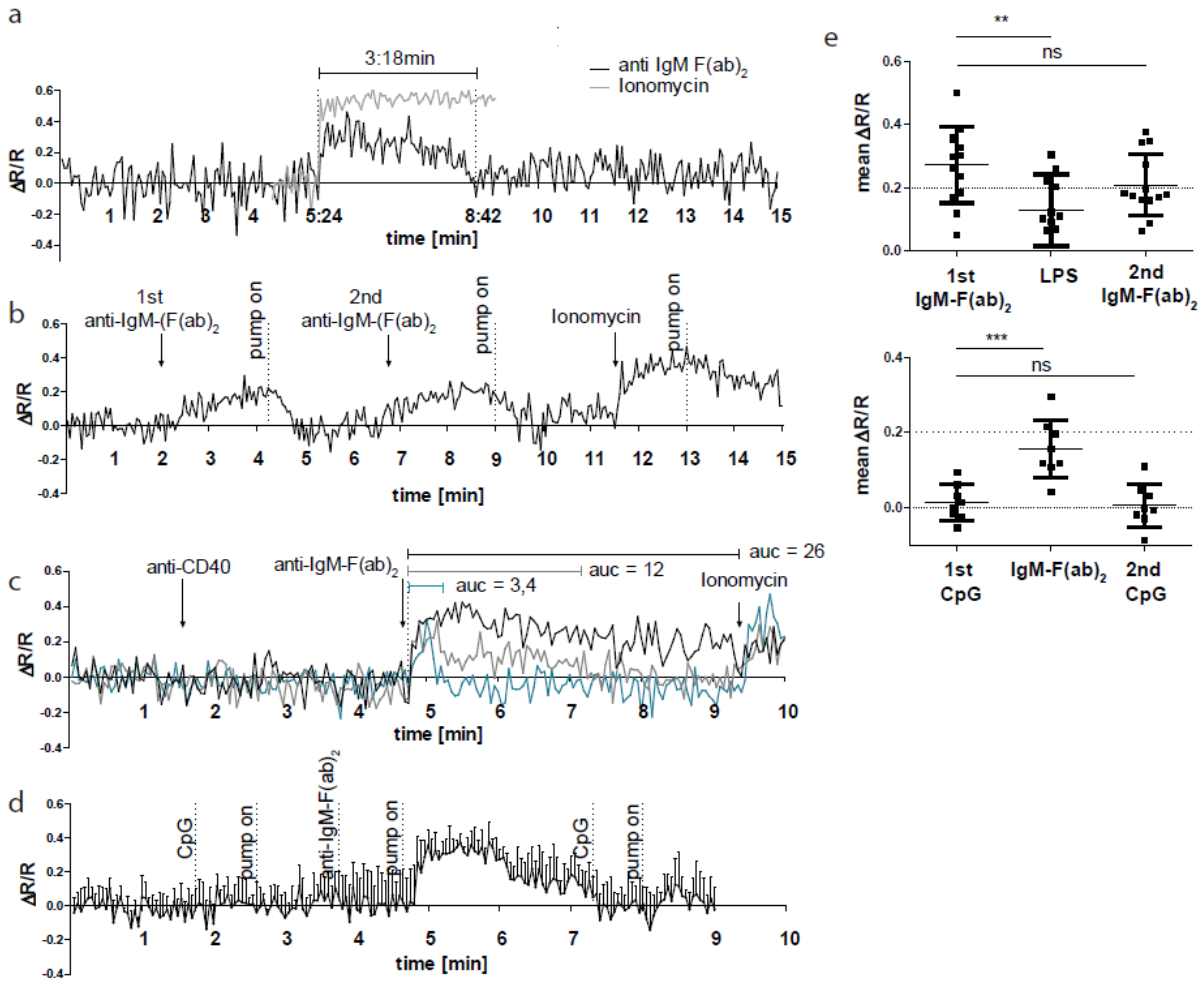

187

188 Fig. 2 BCR stimulation specifically leads to calcium mobilization in YellowCaB cells *in vitro*. a Confocal measurement of FRET
189 duration (ΔR/R>0) in non-perfused primary polyclonal YellowCaB cells after addition 10µg/ml anti-IgM-F(ab)$_2$ (black),
190 Ionomycin control (grey). Data representative for at least 35 single cells in four independent experiments. b Confocal
191 measurement of FRET signal change after repeated addition of anti-IgM-F(ab)$_2$ to perfused primary polyclonal YellowCaB
192 cells. Data representative for at least 50 cells out of five independent experiments. c Confocal measurement of FRET signal
193 change after addition of anti-IgM-F(ab)$_2$ to perfused primary polyclonal YellowCaB cells following stimulation with anti-
194 CD40 antibody and Ionomycin positive control. Examples of transient cytoplasmic (blue), intermediate (grey) and sustained
195 calcium mobilization shown, area under the curve (AUC) compared. Data representative for 26 cells out of two independent
196 experiments. d Resulting FRET curve out for n=7 primary polyclonal YellowCaB cells perfused with TLR9 stimulator CpG in
197 Ringer solution and subsequent addition of anti-IgM-F(ab)$_2$. e Mean FRET signal change over time after addition of TLR4 or
198 TLR9 stimulation in combination with BCR crosslinking by anti-IgM-F(ab)$_2$ in perfused polyclonal YellowCaB cells n=12
199 (upper) and n=8 (lower) **: p=0.0086, ***: p<0.05, one-way ANOVA. Error bars: SD/mean.

200 **Fluctuating calcium levels are observed *in vivo***

201 We next set out to investigate if the ability of B cells to collect calcium signals is also shared
202 by germinal center B cells, and to identify the spatial distribution of possible BCR-triggering
203 forces in an *in vivo* setting. For two-photon intravital imaging, nitrophenyl (NP)-specific B1-
204 8hi:YellowCaB cells were transferred into wild type hosts which were subsequently
205 immunized with NP-CGG (chicken gamma globulin) into the right foot pad[22]. Mice were
206 imaged at day 8 p.i. when GCs had been fully established. Activated TN-XXL$^+$ YellowCaB

207 cells had migrated into the GC and, as confirmed by positive PNA- and anti-GFP
208 immunofluorescence histology (Fig 3 a). At this time point, mice were surgically prepared for
209 imaging as described before[23]. Briefly, the right popliteal lymph node was exposed,
210 moisturized and flattened under a cover slip sealed against liquid drainage by an insulating
211 compound. The temperature of the lymph node was adjusted to 37°C and monitored during
212 the measurement. Our experiments revealed that the movement of single YellowCaB cells
213 can be tracked *in vivo. C*alcium fluctuations can be made visible by intensity changes in an
214 extra channel that depicts the FRET signal, as calculated from relative quenching of TN-XXL.
215 Color-coding of intensity changes in the FRET channel showed time-dependent fluctuations
216 of the signal and, in some particular cases, a sustained increase after prolonged contacts
217 between two YellowCaB cells (Fig 3 b, movie S1). Interestingly, FRET intensity seemed to be
218 mostly fluctuating around low levels in moving cells, whereas sustained increase required
219 cell arrest (Fig S3). We already showed that signal changes in FRET of TN-XXL are
220 reflecting BCR activation. The observed calcium fluctuations might therefore coincide with
221 cell-to-cell contacts between FDCs and B cells, resulting in AG-dependent BCR stimulation.
222 To test for this, we first measured the colocalization between signals within the FDC-channel
223 and the citrine channel. The intensity of colocalization I_{coloc} of all cells was plotted as a
224 function of frequency and biexponentially fitted (Fig 3 c). We set the threshold for a strong
225 and sustained colocalization of FDCs and B cells to an intensity of 150 AU within the
226 colocalization channel. At this value, the decay of the biexponential fit was below 10%. We
227 thus decided to term all cells with a colocalization intensity = 0 (naturally the most abundant
228 ones) not colocalized, cells with a colocalization intensity between 1 and 150 transiently
229 colocalized to FDCs ("scanning" or shortly touching the FDCs) and all cells above this
230 intensity threshold strongly or stably colocalized. When we compared the relative FRET
231 intensity changes ΔR/R of a tracked cell (Fig 3 b, cell 1), where baseline R is the lowest
232 FRET intensity measured, and its contacts to FDCs, we could indeed detect several transient
233 B-cell-FDC contacts that were followed by a step-wise increase of ΔR/R and thus an
234 increase of cytoplasmic calcium concentration (Fig 3 d). These increases in B cells were not
235 only restricted to contacts with FDCs, but also occurred between B cells: A visible contact of
236 cell 1 (Fig 3 b, cell 1) to a fellow B cell (Fig 3 b, cell 2) caused a sustained boost of the
237 calcium concentration in the tracked cell 1 (Fig 3d). Cell 2 itself kept strong FDC contact over
238 the whole imaging period and maintained elevated, but mostly stable ΔR/R values. These
239 experiments confirmed that GC B cells are able to collect calcium as a consequence of
240 repeated signaling events mediated by FDC-to-B cell contacts and, surprisingly, also by B-to-
241 B cell contacts *in vivo*.

242 Next, we asked if the ability to perform BCR signaling is dependent on BCR affinity. Thus, we
243 adoptively transferred stained polyclonal, non-AG-specific YellowCaB cells one day prior to

intravital imaging and compared FRET-signal changes of several tracked cells over time within the same measurement. Non-AG-specific YellowCaB cells showed a rather homogenous distribution of calcium concentration with low intensity fluctuations in the FRET channel around a mean of 13.88 AU, whereas AG-specific YellowCaB cells showed heterogeneous signaling patterns with higher FRET intensities of 14.25 AU on average (Fig. 3e). We compared ratiometric FRET histograms of non-AG-specific and AG-specific cells out of five different measurements. To do so, we normalized FRET values by the mean fluorescence intensity averaged over all non-AG-specific YellowCaB cells. This further confirmed a positive correlation of B cell calcium concentration and BCR-affinity (Fig S4).

Absolute quantification of cytoplasmic calcium by eCFP fluorescence lifetime analysis reveals activation-dependent calcium heterogeneity in B cells

Due to varying imaging depths and therefore differing noise levels in tissue, the comparison of measurements in a ratiometric set-up only gives relative information about calcium concentrations. Therefore, universal statements on calcium levels among different B cell populations will demand absolute quantification. We switched our imaging set-up from the analysis of the fluorescent intensities of eCFP and citrine to the measurement of the fluorescence lifetime (tau) of the FRET-donor eCFP. Fluorescence lifetime is defined as the mean time a fluorescent molecule stays in an elevated energetic state after excitation, before photon emission and relaxation to the ground state take place. As a fully calcium-quenched eCFP in the GECI TN-XXL would transfer its energy mainly to citrine, its fluorescence lifetime would be measurably shorter than on an unquenched eCFP. Phasor analysis of time-domain FLIM virtually transfers time-resolved fluorescence data into phase domain data by discrete Fourier transformation[14]. This approach overcomes the obstacles of multi-component exponential analysis and yields readily comparable pixel- or cell based plots that assign a position within a half-circle to each data point, dependent on the mixture of lifetime components present[24].

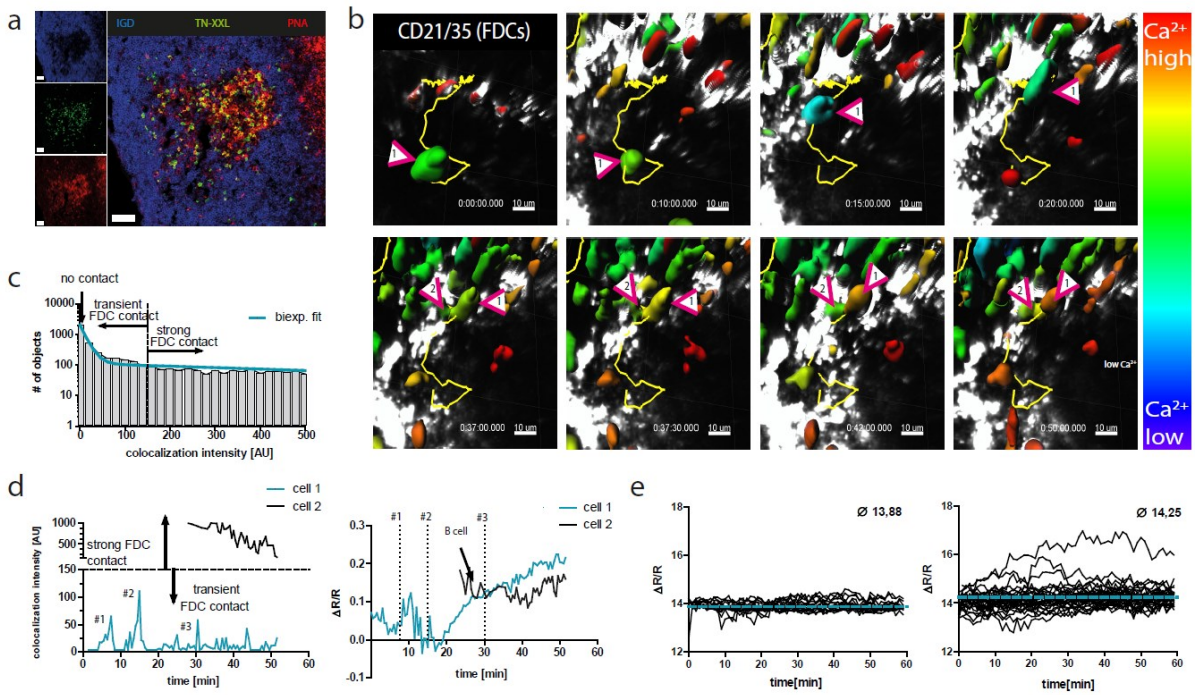

Fig. 3 YellowCaB cells form productive germinal centers in vivo and show active BCR signaling after cell-to-cell contacts. a Histological analysis of lymph nodes after adoptive transfer of polyclonal YellowCaB cells to restricted hosts. TN-XXL (green) positive cells cluster in IgD (blue) negative regions and are showing activation, confirmed by PNA staining (red). Scale bar 50µm. b Stills of intravital imaging of polyclonal YellowCaB cells transferred to restricted host. 3D surface rendering and single-cell tracking (track line in yellow) with relative color coding ranging from blue= low ΔR/R to red=high ΔR/R c Histogram showing cell frequency vs. colocalization intensity [AU] and biexponential fit of data. A curve decay of <10% was set as threshold parting transient from strong B cell-to-FDC contact. All cells with colocalization intensity <1 were assigned negative. d Colocalization intensities of tracked cells 1 and 2 over time vs FRET signal change of cell 1 and 2 over time. Contact events to FDCs are assigned numbers #1, #2 and #3. Contact between cell 1 and 2 is indicated by arrow. e Comparison of FRET signal change of naive and AG-specific YellowCaB cells over time.; blue line indicates mean value of all tracked cells n=16 (naive) and n=33 (AG-spec.).

Employing our adoptive cell transfer set up described above (Fig 4 a), we could divide GC B cells into five different populations based on their location in the imaging volume and their fluorescent appearance. At day 8 p.i., polyclonal YellowCaB cells, identified by their red labeling, mostly lined up at the follicular mantle around the GC, with some of them having already entered into activated B cell follicles. AG-specific, citrine-positive B1-8hi:YellowCaB cells were found clustered in the GC, close to FDCs, outside of GC boundaries, or as bigger, egg-shaped differentiated cells in the extrafollicular medullary cords (MC), probably comprising plasma blasts (Fig. 4 b). Color-coded 2D and 3D FLIM analysis of these populations confirmed that calcium concentrations were fluctuating within all of those B cell populations, and that most B cells were maintaining relatively high fluorescence lifetimes and therefore low calcium concentration on average with single-cell exceptions (Fig. 4 b, movie S2). It should be noted that autofluorescence of the capsule or macrophages contributed to tau values <800ps, indicated by dark red color-coding and is not to be attributed to high calcium values. Phasor analysis and plotting of the B cell-wise segmented lifetime data further confirmed the presence of cell clones with quenched TN-XXL, somewhat surprisingly

also among plasma blasts, which are thought to down-regulate their surface BCR (Fig 4c, movie S3). To translate the measured lifetime values into absolute calcium concentrations, we projected the data points onto the phasor connecting quenched and unquenched eCFP (Fig. 4d). In this way, we corrected for artifacts acting on the phasor vectors and, implicitly, on the fluorescence lifetimes caused by contribution of background noise (Fig S5). Comparison of AG-specific cells inside GCs with those outside GCs, and non-AG-specific cells inside GCs as well with those outside GCs showed that the distribution of calcium concentrations of these B cells were dependent on BCR specificity and rather independent from their location within the imaging volume, despite higher fluctuation seen among AG-specific populations (Fig S5). However, we noted the emergence of a cell subset that is high in calcium and therefore located on the right half of the plot, in AG-specific cells and most prominent among cells within the MC, as compared to non-AG-specific YellowCaB cells. Overlay of an imaging snapshot shows that only few cells are in a state of elevated calcium (>800 nM) at one given time point (Fig. 4e). Accordingly, these maxima were reached as transient fluctuation peaks, i.e. periods of below one minute, in which these concentrations seem to be tolerated. Calcium values exceeding the dynamic range of TN-XXL (>857nM) were recorded for all measured subsets, but the most cells >857nM were found among intrafollicular AG-specific B cells and extrafollicular AG-specific B cells. (Fig. 4f). The heterogeneity in temporal calcium concentrations therefore is smallest among non-AG specific B cells, increases with activation in AG-specific GC B cells, and is most prominent among plasma blasts. Thus, a progressive heterogeneity of calcium signals within B cells can be seen alongside the process of activation and differentiation.

Functional relevance of increased calcium concentration among extrafollicular YellowCaB cells

The surprising finding of elevated cytoplasmic calcium levels in extrafollicar B cells led us to analyze this subset further. Recently, contacts with subcapsular sinus macrophages (SCSM) were reported to induce the differentiation of memory B cells to antibody producing plasma cells[25–27]. To test, if SCSM could be the cause of elevated extrafollicular calcium levels in differentiated, extrafollicular B cells, we . intravitally imaged wild type host mice that have been adoptively transferred with B1-8hi:YellowCaB cells and received an injection of efluor660-labeled anti-CD169 antibody together with the usual FDCs labeling one day prior to analysis. We concentrated on the area beneath the capsule, identified by second harmonic generation signals of collagen fibers in this area. Thresholds of colocalization between $CD169^+$ macrophages and $TN\text{-}XXL^+$ YellowCaB cells are described in Fig S6. Together, these methods led to the 3D visualization of the SCS with CD169 stained macrophages, lined up in close proximity. (Fig5a). AG-specific YellowCaB cells were

334 detected clustering in GCs nearby. Extrafollicular YellowCaB cells crowding the SCS space
335 were found to have multiple contact sites to SCSM. Some B cells were observed to migrate
336 along the SCS, possibly scanning for stimulatory signals like antigen (movie S4). Cell
337 tracking and simultaneous analysis of absolute calcium concentration and colocalization
338 intensity revealed that B-cell-to-SCSM contacts resulted in an immediate increase in
339 cytoplasmic calcium concentration. In line with this, the loss of a transient-made contact
340 directly leads to a decrease in calcium concentration (Fig 5b). This was further confirmed by
341 bulk analysis of all detected YellowCaB cells over the whole imaging period (Fig 5c). Relating
342 calcium concentration and colocalization showed that the calcium concentration in
343 YellowCaB cells with direct contact to SCSM reaches values that are more than doubled
344 compared to that in cells that were not in contact Furthermore, calcium concentration
345 increase seems to be positively correlated to B cell-to-SCSM contact strength. Co-
346 localization intensities between 0 and 1 were defined as no-contact. All values above
347 describe transient or strong contact. The threshold between transient and strong contact has
348 been set to 10% decay of the biexponentially fitted histogram over all cells. Cells that were
349 defined as strong contacters also reached the highest calcium concentrations. We conclude
350 that contacts of B cells to SCSM could induce elevation of B cell cytoplasmic calcium
351 concentrations, presumably due to activation, with the absolute concentrations being
352 dependent on the strength of the contact.

353

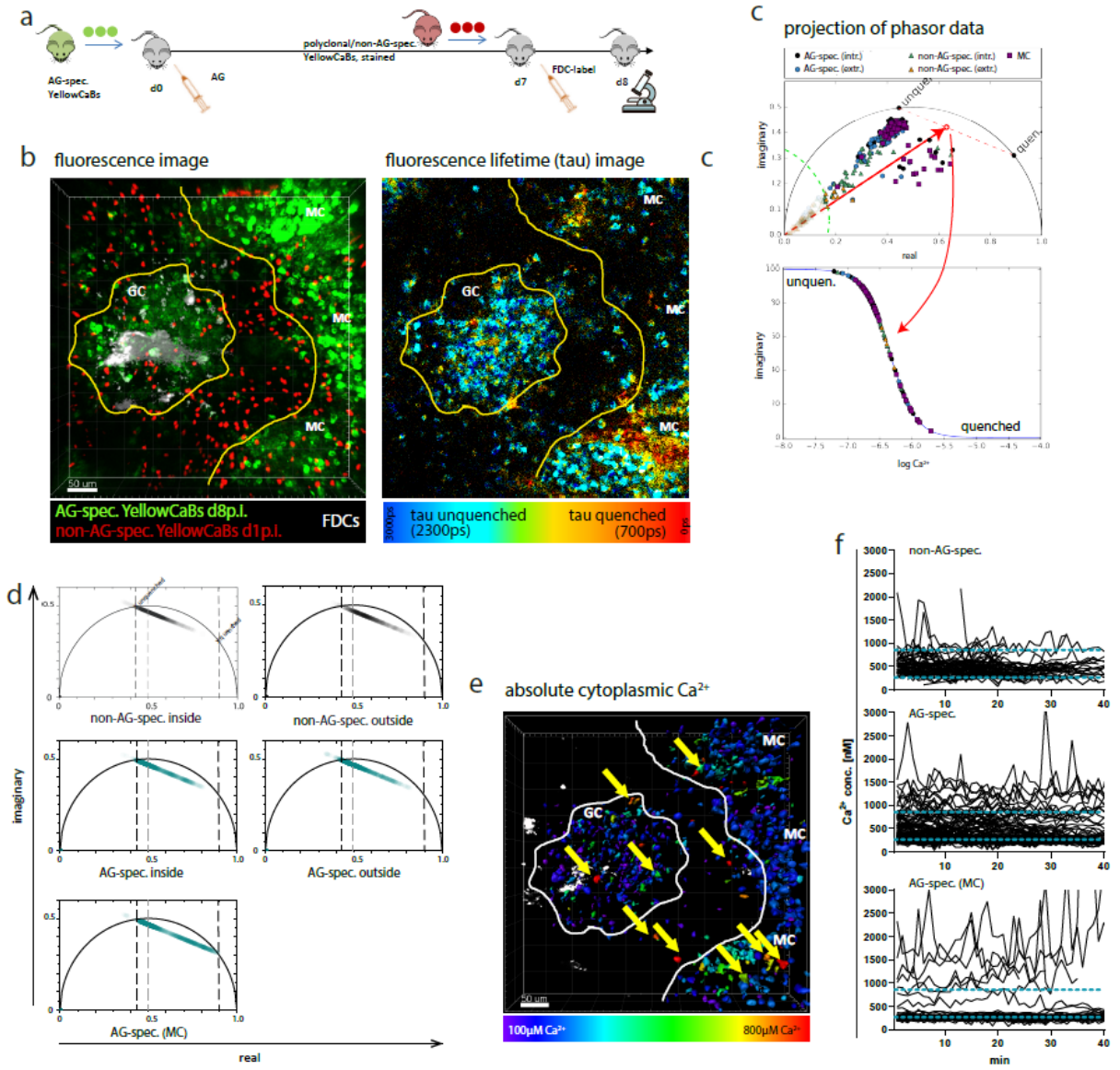

Fig. 4 Determination of absolute calcium concentration by intravital fluorescence lifetime imaging of GC B cell populations. a Cell transfer and immunization strategy for intravital imaging of AG-specific and polyclonal YellowCaB B cells. b z-stack of intravitally imaged germinal center (GC) and medullary cords (MC). B cells have been distinguished into polyclonal, non-AG-specific YellowCaB cells (red) inside and outside the germinal center, AG-specific YellowCaB cells inside and outside the germinal center and differentiated B cells (plasma blasts) due to staining and localization (left). Color-coded fluorescence lifetime image (right) with lifetimes of unquenched eCFP depicted in blue and lifetimes of quenched eCFP in red. c Phasor plot of fluorescence lifetimes measured in b with indicated subpopulations. Green radius indicates noise that has been excluded from the evaluation of absolute calcium concentrations. For absolute calcium concentration determination, phasors of single cells have been projected to the red-dashed line connecting fully calcium-saturated (quenched) and calcium-free (unquenched) conditions d Projections of phasor vectors onto connecting line between unquenched and quenched eCFP lifetimes among the different subpopulations. f calcium concentrations intravitally measured with FLIM-phasor in germinal center B cell populations over time. Non-AG-specific YellowCaB cells (left, n=92) compared to AG-specific YellowCaB cells (middle, n=169) and extrafollicular, AG-specific YellowCaB cells (right, n=69) The dynamic range of the GECI TN-XXL is indicated by blue dashed lines.

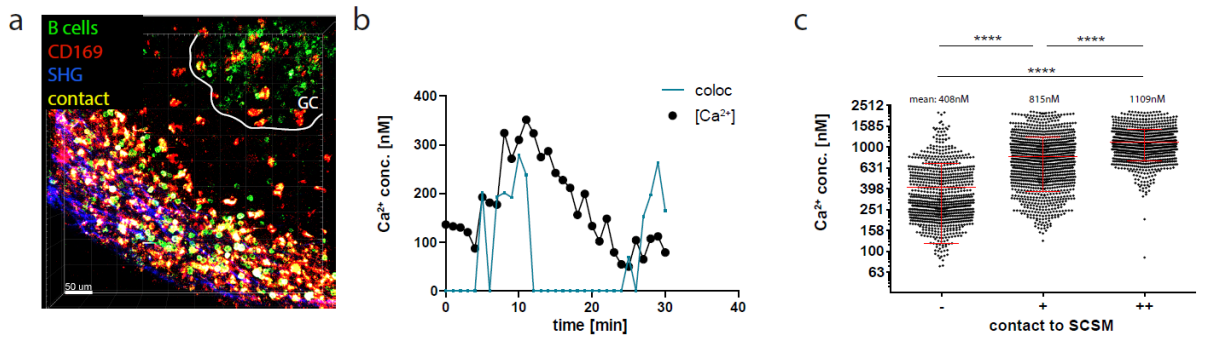

Fig. 5 Differentiated B cells show elevated calcium concentrations after contact to macrophages of the subcapsular sinus. a z-stack of intravitally imaged lymph node with germinal center (GC) and subcapsular sinus (SHG, blue). CD169^{+} macrophages (red) lining the subcapsular sinus show large contacts (yellow) to YellowCaB cells (green) of increased brightness and size that therefore have been identified as differentiated B cells. Size 500x500x78µm. Scale bar 60µm. b Single-cell track of a YellowCaB cell making transient contact to macrophage, blue: colocalization intensity [AU], black: change of absolute calcium concentration. c FLIM measurement of mean absolute calcium concentration of YellowCaB cells showing no (-), transient (+) or strong (++) overlap with CD169^{+} signal. n=1000, ANOVA analysis (****: $p<0.0001$), mean and SD.

Discussion

Intravital imaging technologies have helped to elucidate the nature of the GC reaction a great deal. AG-capture, cycling between zones, and development of clonality patterns have been made visible by two-photon microscopic techniques[5,28–30]. Furthermore, important functional *in vivo* data like signaling in T helper cells have been collected using a calcium sensitive protein[31,32].

Research on signaling of (GC) B cells *in vivo* so far involved transfer and immunization experiments and *ex vivo* analysis of sorted cells, or used non-reversible BCR-signaling reporters like Nur77[10,33,34]. These experiments led to the conclusion that only a small amount of GC B cells seem to maintain the signaling capacity of naive, mature B cells and that BCR signaling thus is dispensable in GCs[10,11,35–38]. On the other hand, BCR-regulating surface proteins like CD22 or Sialic acid-binding immunoglobulin-type lectins (Siglecs) have been related to development of autoimmunity and point out to BCR signaling as an important component, not only in B cell development but also in differentiation to effector cells[39–42].

We here show the establishment of a novel transgenic reporter system and image processing approach, enabling – for the first time - B cell cytoplasmic calcium quantification *in vivo*. We show that the FRET-based GECI TN-XXL can be used stably in moving, proliferating and differentiating lymphocytes. The reversibility of the sensor makes it suitable for longitudinal measurements. Perfused YellowCaB cell culture set ups furthermore allow for flexible manipulation of receptor stimulation.

399 By measuring calcium flux within B cells in vitro, we could show fast reversibility and suitable
400 sensitivity of the GECI TN-XXL for intravital applications. Using a flow chamber system, we
401 could show that repeated BCR activation leads to repeated calcium elevation in the
402 cytoplasm. Thus, our system shows that B cells are able to collect and integrate sequential
403 signals, probably for positive selection, acting via calcium accumulation up to a hypothetic
404 threshold. In support of that, B cellular calcium concentration must not constitutively exceed
405 a certain value in order to prevent mitochondrial depolarization[43,44] On the other hand, it is
406 known that certain elevated calcium concentrations and timely regulated calcium flux
407 patterns decide if and which downstream transcription factors are activated[45,46]. Balancing
408 out calcium concentrations might thus also function in sensing the completion of affinity
409 maturation. We propose calcium fluctuation as time- and strength-coded system for the
410 transduction of information about growing BCR affinity. Fine-tuned signaling mechanisms are
411 well known for other signaling types and partly instruct conflicting transcriptional
412 mechanisms; e.g. CD40 signaling is absolutely indispensable for entry of B cells into the GC
413 reaction, but prolonged CD40 signaling instead promotes IRF4 transcription and therefore
414 favors an extrafollicular ASC phenotype[47].

415 *In vivo* imaging of different B cell subsets with growing heterogeneity further suggests a
416 correlation between cytoplasmic calcium concentrations and selection. We found that
417 differentiated extrafollicular B cells or plasma blasts are among the cells with highest calcium
418 concentrations within our set up. Moreover, high calcium concentrations might also act as
419 stress signal that demands restriction. Recent reports state that elevated calcium might set a
420 "metabolic timer" for T cell help to rescue a mitochondria-depolarizing ion concentration[48].
421 This shows that calcium levels within cells need to be tightly regulated, as it does also play
422 its part in the induction of apoptosis. Calcium levels of >1 µM over the duration of >1 h have
423 been reported damaging in neurons[49,50]. Since apoptosis is the default cell fate for B cells in
424 the germinal center reaction[51], CD40 and TLR signaling might contribute to the limiting of
425 cytoplasmic calcium concentrations and thus promote cell survival of B cell clones with
426 appropriate BCR affinity[21,52–55]. For CD40 signaling in immature B cells this has been
427 confirmed[56]. Our data does show that TLR signaling can attenuate calcium flux in stimulated
428 B cells, CD40 can either attenuate or augment the calcium response, presumably depending
429 on the affinity of the BCR and its efficiency in presenting AG[29,32].

430 We show, that within GCs, FDCs or other B cells can stimulate calcium flux, the latter
431 possibly being explained by simultaneous stimulation of BCRs and Fc receptors[57–61].
432 Whether this activation in terms of calcium mobilization is further modulated by T helper cells
433 *in vivo*, still needs to be determined by imaging AG specific T-B interactions in our system.

434 We were able to image ongoing cytoplasmic calcium elevation in the regions of the MC or
435 the subcapsular sinus and confirmed elevated calcium concentrations in B cells in contact to
436 SCSM. The latter has recently been proposed as site of reactivation of memory B cells[25].
437 Whether these changes are due to residual BCR signaling in these subsets, needs to be
438 investigated.

439 We created a technique that paves the way for functional studies of living cells, and
440 unleashes the use of FRET in intravital microscopy, a neglected potential due to the
441 challenges that deep tissue imaging imposes. We could visualize that B cell differentiation is
442 a process of repeated activation via BCR- and costimulatory signals that stem from serial
443 contacts of B cells with AG provided by other cells. Using time-resolved FRET-FLIM
444 measurements in GC, we could show that BCR AG-specificity and state of differentiation are
445 closely related to distinct degrees of heterogeneity of calcium concentrations. While it is
446 worthwhile noting that the cells imaged within the MC region most likely comprise of
447 extrafollicularly generated plasma blasts, rather than differentiated B cells that have left the
448 GC (these are reported to appear only at much later stages of the response), we are
449 confident that our set-up models different B cell activation and differentiation stages in a
450 single measurement[62]. We suggest that during differentiation, calcium signals mainly act as
451 transcriptional regulators. Within already differentiated cells, one possible downstream effect
452 of elevated calcium could be changes in mitochondrial membrane potential and/or the
453 integrity of the ER, since both act as major intracellular calcium buffering organelles[63]. A
454 close connection between mitochondrial calcium homeostasis, altered ROS production and
455 the expression of plasma cell master transcription factor BLIMP1, as well as changes in
456 metabolism have been reported previously[64,65]. We have already applied phasor-FLIM of
457 endogenous NAD(P)H fluorescence for mapping of enzyme activities in cell cultures62. The
458 application of this method and combination with calcium imaging holds great potential to
459 further dissect immunometabolic processes in B cells, short- and long-lived plasma cells *in*
460 *vivo*.

461 **Methods**

462 Mice

463 PR26CAGTN-XXL$^{flox/flox}$ mice were obtained by courtesy of F. Kirchhoff, Saarland University,
464 Homburg[66]. YellowCaB mice were generated by crossing of R26CAGTN-XXL$^{flox/flox}$ mice with
465 the CD19$^{cre/cre}$ strain[16] and maintained on a C57/Bl6 background. Only YellowCaB mice
466 heterozygous for cre were used to avoid deletion of CD19. Mice with monoclonal NP-specific
467 BCR (B1-8^{hi}:YellowCaB) were generated by crossing of YellowCaB mice with B1-8^{hi} mice[22].
468 Thx mice were used as irrelevant-BCR hosts. All mice were bred in the animal facility of the

469 DRFZ. All animal experiments were approved by Landesamt für Gesundheit und Soziales,
470 Berlin, Germany, in accordance with institutional, state, and federal guidelines.

471 Cells

472 Primary splenocytes were isolated from whole spleens of YellowCaB mice or
473 B1-8^{hi}:YellowCaB mice in 1xPBS and erythrocytes lysed. B cells were negatively isolated
474 using the Miltenyi murine B cell isolation kit via magnetic assisted cell sorting (MACS) leave
475 B cells untouched in order not to pre-stimulate them.

476 Staining and flow cytometry

477 To simultaneously assess calcium influx with a dye-based method we stained whole
478 splenocytes or isolated B cells with the calcium sensitive dye X-Rhod-1 (invitrogen). X-Rhod-
479 1 is a single-fluorophore calcium reporter molecule that enhances its fluorescence intensity
480 upon calcium binding in a range of 0-40 µM up to 100 times at a wavelength of 600nm.
481 Measurements were carried out at a BD Fortessa flow cytometer. TN-XXL expression was
482 checked assessing positive fluorescence in a 525±25 nm channel after 488nm excitation on a
483 MACSQuant flow cytometer.

484 Perfusion chamber

485 All *in vitro* experiments were carried out in Krebs-Ringer solution containing 6mM Ca^{2+} at
486 37°C. Cells were stimulated with anti-mouse IgM-F(ab)$_2$ (Southern Biotech), ionomycin (4µM,
487 Sigma), anti-CD40 antibody (xy), LPS (20 µg/ml, Sigma) or CpG (10 µg/ml, TIB Molbiol
488 Berlin). Cell culture imaging experiments with ionomycin stimulation were performed using an
489 open perfusion chamber system. Buffer solution was pumped through the heated chamber
490 containing a poly-D-Lysin coated glass slide on which freshly and sterile isolated YellowCaB
491 cells were grown for approx. 1 h. Ionomycin was added in the flow-through buffer supply. The
492 lag time for the volume to arrive at the imaging volume was determined for each set-up and
493 considered for analysis of ΔR/R over time. Anti-IgM-F(ab)$_2$ antibody was given directly to
494 cells within the open chamber in between acquisition time points. To visualize the reversibility
495 of the sensor despite antibody still present, the experiment was performed in an open culture
496 system without media exchange through a pump. To analyze if YellowCaB cells could
497 repeatedly be stimulated, experiments were performed under continuous perfusion. Buffer
498 flow was switched off with stimulation for several minutes and switched on again to dilute
499 antibody out again for a second stimulation.

500 For analysis, regions of interest were determined based on randomly chosen single cells.
501 Intensity density values of the raw citrine signal were divided by the intensity density values
502 of the raw eCFP signal and related to the baseline ratio of the signals before stimulation.

503 Cell transfers, immunization and surgical procedures

504 B cells from spleens of YellowCaB mice were negatively isolated using the Miltenyi murine B
505 cell isolation kit via MACS. $5x10^6$ cells were transferred to a host mouse with a transgenic B
506 cell receptor specific for an irrelevant antigen (myelin oligodendrocyte glycoprotein). B cells
507 from spleens of B1-8^{hi}:YellowCaB mice were transferred to WT C57/Bl6 mice. Host mice
508 were immunized in the right footpad with 10 µg NP-CGG in complete Freund's adjuvant 24h
509 after B cell transfer. After six to eight days p.i., FDCs were labeled with Fab-Fragment of
510 CD21/35-Atto590 or CD21/35-Alexa647 (inhouse coupling) into the right footpad. 24h after
511 labelling, the popliteal lymph node was exposed for two-photon-imaging as described
512 before[23]. Briefly, the anesthetized mouse is fixed on a microscope stage custom-made for
513 imaging the popliteal lymph node. The mouse is shaved and incisions are made to introduce
514 fixators that surround the spine and the femoral bone. The mouse is thus held in a planar
515 position to the object table. The right foot is fixed by wire allowing to increase the tension on
516 the leg to position the lymph node parallel to the imaging set up. A small incision is made to
517 the popliteal area. The lymph node is exposed after freeing it from surrounding adipose
518 tissue. A puddle around the lymph node is formed out of insolating silicon compound, then
519 filled with NaCl and covered bubble-free with a cover slide.

520 Intravital and live cell imaging and image analysis

521 Imaging experiments of freshly isolated B cells were carried out using a Zeiss LSM 710
522 confocal microscope. Images were acquired measuring 200-600 frames with 1 frame/3s
523 frame rate while simultaneously detecting eCFP and citrine signals at an excitation
524 wavelength of 405 nm.

525 For intravital two-photon ratiometric imaging, Z-stacks were acquired over a time period of
526 30-50 min with image acquisition every 30 seconds. eCFP and citrine were excited at 850nm
527 by a fs-pulsed Ti:Sa laser and fluorescence was detected at 466±30 nm or 525±25 nm,
528 respectively. Fluorescence signals of FDCs were detected in a 593±20 nm channel. For
529 experiments including macrophage-staining, the fluorescence data has been unmixed for a
530 possible overlap of the TN-XXL-citrine signal with that of the injected marker to prevent false-
531 positive colocalization analysis between the red efluor660 coupling of anti-CD169 and the
532 green fluorescence of TN-XXL in the 525±25nm channel[67].

533 For intravital FLIM experiments, eCFP fluorescence lifetime was measured with a time-
534 correlated single-photon counting system (LaVision Biotec, Bielefeld, Germany). The
535 fluorescence decay curve encompassed 10 ns with a time resolution of 55 ps and is a bi-
536 exponential function containing the two mono-exponential decays of unquenched CFP and of
537 FRET-quenched CFP, respectively.

538 Analysis of two-photon data

539 For ratiometric analysis of two-photon data (here the exciting wavelength of 850 nm is also
540 stimulating citrine fluorescence directly), fluorescence signals were corrected for spectral
541 overlap (the eCFP to citrine ratio in 525±25 nm channel is 0.52/0.48) and refined by taking
542 into account the sensitivity of photomultiplier tubes (PMTs, 0.37 for 466±30 nm and 0.4 for
543 525±25 nm). Ratiometric FRET for in vivo experiments was accordingly calculated as

544 $$FRET = \frac{1{,}2 \cdot ch2}{2{,}7 \cdot ch1 + 2{,}5 \cdot ch2} \cdot 100 \quad \text{(Eq. 1)}$$

545 Evaluation of FLIM data was performed using the phasor approach[14,24]. Briefly, the
546 fluorescence decay in each pixel of the image is Fourier-transformed at a frequency of
547 80 MHz and normalized, resulting into a phasor vector, with the origin at (0|0) in a cartesian
548 system, pointing into a distinct direction within a half-circle centered at (0.5|0) and a radius of
549 0.5. For pure substances, lifetime vectors end directly on the half-circle, for mixtures of two
550 on a connecting line between the respective pure lifetimes and within a triangle, if three
551 substances are present, and so on. The distance between several fluorescence lifetimes on
552 the half-circle is naturally distributed logarithmically, with the longest lifetimes closer to the
553 origin. In the case of TN XXL, the extremes are the unquenched CFP fluorescence (2300 ps)
554 and the CFP fluorescence completely quenched by FRET (700 ps). The location of the
555 measured lifetime on the connecting line can directly be translated into the amount of either
556 CFP state and thus to a corresponding calcium concentration.

557 Due to the scattering environment in tissue, the FLIM-signal of the donor is shifted towards
558 the (0/0) position in the phasor plot, indicative for the infinite lifetime of noise. Thus the phase
559 vectors are shortened and end within a triangle between the points (0|0), approximately
560 2300 ps and 700 ps. The noise should therefore be considered as a contribution of a third
561 exponential component. In a non-fluorescent medium, we measured a noisy FLIM-signal
562 under similar experimental conditions as those used in the intravital experiments and
563 Gaussian-fitted the histograms of real and imaginary part after the transformation to the
564 frequency domain. The Gaussian fit of each part gives a mean, which indicates the center of
565 the noise distribution, as wells as the width ($FWHM = 2\sqrt{2ln2}\sigma$), which was the same for
566 both parts (real and imaginary axis) and gives us the radius (½FWHM = 0.2 (green, solid arc
567 in Fig. S5) within which we expect only noise, i.e. the signal-to-background-ratio is unreliable
568 small. In order to increase the accuracy, we enlarged the radius to ¾FWHM = 0.3 (green,
569 dashed arc in Fig. S5) and all data points within that radius were excluded from further
570 analysis. A second filtering was applied by determining the signal-to-noise ratio (SNR) from
571 the summed TCSPC signal for all segmented cells. In Imaris, a sphere of radius=20µm was

572 determined around each cell to establish a reference value for background noise. The SNR
573 was then calculated as follows (pixel by pixel):

574 $$\frac{I_{sig}-I_{bg}}{STD_{bg}} \text{ (Eq. 3)}$$

575 With I_{sig} being the intensity of TCSPC signal, I_{bg} the intensity of background noise and STD_{bg}
576 the background noise standard deviation[68] AG specific signals with SNR<2 and non-Ag
577 specific signals with SNR<1 were excluded from the analysis. All other phasor data points
578 were projected on the segment connecting FRET-quenched and unquenched CFP
579 fluorescence lifetime, in order to determine absolute calcium concentrations as follows:

580 $$log[Ca^{2+}] = logK_d + 0.2 \cdot ln\left[\frac{2300-700}{\tau-700} - 1\right] \qquad \text{(Eq. 2)}$$
581

582 with Kd = 453 nM calcium[15]. The linear range of the TN-XXL titration curve was determined to
583 be 265nM-857nM. All values below or above these margins are subject to uncertainty and
584 therefore simply referred to as <265nM or >875nM, respectively.

585 **Statistical information**

586 Time dependent FRET curve analysis shows representative graphs for the number of
587 analyzed cells and independent experiments given. For multiple curve analysis, mean is
588 shown and SD indicated in each data point. For column analysis, One-way ANOVA with
589 Bonferroni Multiple Comparison Test was applied with a confidence Interval of 95%.

590 **Data availability**

591 All raw data and analyzed data shown here are stored on institutional servers and may be
592 accessed upon request to the corresponding author.

593 **Code availability**

594 Python-based code for phasor analysis can be provided upon request.

595 **References**

596 1. Victora, G. D. & Nussenzweig, M. C. Germinal Centers. *Annu. Rev. Immunol.* **30**, 429–
597 457 (2012).

598 2. Berek, C., Berger, a. & Apel, M. Maturation of the immune response in germinal
599 centers. *Cell* **67**, 1121–1129 (1991).

600 3. De Silva, N. S. & Klein, U. Dynamics of B cells in germinal centres. *Nat. Rev.*

601 *Immunol.* **15**, 137–148 (2015).

602 4. Tolar, P., Hanna, J., Krueger, P. D. & Pierce, S. K. The constant region of the
603 membrane immunoglobulin mediates B cell-receptor clustering and signaling in
604 response to membrane antigens. *Immunity* **30**, 44–55 (2009).

605 5. Suzuki, K., Grigorova, I., Phan, T. G., Kelly, L. M. & Cyster, J. G. Visualizing B cell
606 capture of cognate antigen from follicular dendritic cells. *J. Exp. Med.* **206**, 1485–1493
607 (2009).

608 6. Su, T. T. *et al.* PKC-β controls IκB kinase lipid raft recruitment and activation in
609 response to BCR signaling. *Nat. Immunol.* (2002). doi:10.1038/ni823

610 7. Saijo, K. *et al.* Protein Kinase C β Controls Nuclear Factor κB Activation in B Cells
611 Through Selective Regulation of the IκB Kinase α. *J. Exp. Med.* (2002).
612 doi:10.1084/jem.20020408

613 8. Crabtree, G. R. & Olson, E. N. NFAT signaling: choreographing the social lives of
614 cells. *Cell* (2002).

615 9. Jellusova, J. Cross-talk between signal transduction and metabolism in B cells.
616 *Immunol. Lett.* **201**, 1–13 (2018).

617 10. Luo, W. *et al.* B cell receptor and CD40 signaling are rewired for synergistic induction
618 of the c-Myc transcription factor in germinal center B cells. *Immunity* **48**, 313–326
619 (2018).

620 11. Gitlin, A. D. *et al.* T cell help controls the speed of the cell cycle in germinal center B
621 cells. *Science (80-.).* **349**, 643–646 (2015).

622 12. Akkaya, M. *et al.* Second signals rescue B cells from activation-induced mitochondrial
623 dysfunction and death. *Nat. Immunol.* **19**, 871–884 (2018).

624 13. Mank, M. *et al.* A FRET-based calcium biosensor with fast signal kinetics and high
625 fluorescence change. *Biophys. J.* **90**, 1790–1796 (2006).

626 14. Digman, M. A., Caiolfa, V. R., Zamai, M. & Gratton, E. The phasor approach to
627 fluorescence lifetime imaging analysis. *Biophys. J.* **94**, L14–L16 (2008).

628 15. Geiger, A. *et al.* Correlating calcium binding, Förster resonance energy transfer, and
629 conformational change in the biosensor TN-XXL. *Biophys. J.* **102**, 2401–10 (2012).

630 16. Rickert, R. C., Roes, J. & Rajewsky, K. B lymphocyte-specific, Cre-mediated

631 mutagenesis in mice. *Nucleic Acids Res.* **25**, 1317–1318 (1997).

632 17. Li, N., Sul, J.-Y. & Haydon, P. G. A calcium-induced calcium influx factor, nitric oxide,
633 modulates the refilling of calcium stores in astrocytes. *J. Neurosci.* (2003).

634 18. Baba, Y., Matsumoto, M. & Kurosaki, T. Calcium signaling in B cells: Regulation of
635 cytosolic Ca2+ increase and its sensor molecules, STIM1 and STIM2. *Mol. Immunol.*
636 **2**, 2–6 (2013).

637 19. Ojaniemi, M. *et al.* Phosphatidylinositol 3-kinase is involved in Toll-like receptor 4-
638 mediated cytokine expression in mouse macrophages. *Eur. J. Immunol.* **33**, 597–605
639 (2003).

640 20. Ren, H. *et al.* Toll-like receptor-triggered calcium mobilization protects mice against
641 bacterial infection through extracellular ATP release. *Infect. Immun.* **82**, 5076–5085
642 (2014).

643 21. Pone, E. J. *et al.* B cell TLR1/2, TLR4, TLR7 and TLR9 interact in induction of class
644 switch DNA recombination: Modulation by BCR and CD40, and relevance to T-
645 independent antibody responses. *Autoimmunity* **48**, 1–12 (2015).

646 22. Shih, T.-A. Y., Meffre, E., Roederer, M. & Nussenzweig, M. C. Role of BCR affinity in T
647 cell dependent antibody responses in vivo. *Nat. Immunol.* **3**, 570–5 (2002).

648 23. Ulbricht, C., Lindquist, R. L., Tech, L. M. & Hauser, A. E. Tracking plasma cell
649 differentiation in living mice with two-photon-microscopy. *Methods Mol. Biol.* **1623**, 37–
650 50 (2017).

651 24. Leben, R. *et al.* Phasor-based endogenous NAD(P)H fluorescence lifetime imaging
652 unravels specific enzymatic activity of neutrophil granulocytes preceding NETosis. *Int.*
653 *J. Mol. Sci.* **19**, (2018).

654 25. Moran, I. *et al.* Memory B cells are reactivated in subcapsular proliferative foci of
655 lymph nodes. *Nat. Commun.* **9**, 1–14 (2018).

656 26. Junt, T. *et al.* Subcapsular sinus macrophages in lymph nodes clear lymph-borne
657 viruses and present them to antiviral B cells. *Nature* **450**, 110–114 (2007).

658 27. Von Andrian, U. H. & Mempel, T. R. Homing and cellular traffic in lymph nodes. *Nat.*
659 *Rev. Immunol.* **3**, 867–878 (2003).

660 28. Hauser, A. E. *et al.* Definition of germinal-center B cell migration in vivo reveals
661 predominant intrazonal circulation patterns. *Immunity* **26**, 655–67 (2007).

662 29. Victora, G. D. *et al.* Germinal center dynamics revealed by multiphoton microscopy
663 using a photoactivatable fluorescent reporter. *Cell* **143**, 592–605 (2010).

664 30. Tas, J. M. J. *et al.* Visualizing antibody affinity maturation in germinal centers. *Science*
665 *(80-.).* **58**, 7250–7 (2016).

666 31. Kyratsous, N. I. *et al.* Visualizing context-dependent calcium signaling in
667 encephalitogenic T cells in vivo by two-photon microscopy. *Proc. Natl. Acad. Sci.* **114**,
668 E6381–E6389 (2017).

669 32. Shulman, Z. *et al.* Dynamic signaling by T follicular helper cells during germinal center
670 B cell selection. *Science* **345**, 1058–62 (2014).

671 33. Khalil, A. M., Cambier, J. C. & Shlomchik, M. J. B cell receptor signal transduction in
672 the GC is short-circuited by high phosphatase activity. *Science* **336**, 1178–81 (2012).

673 34. Mueller, J., Matloubian, M. & Zikherman, J. Cutting Edge: An in vivo reporter reveals
674 active B cell receptor signaling in the germinal center. *J. Immunol.* **194**, 2993–7
675 (2015).

676 35. Zikherman, J., Parameswaran, R. & Weiss, A. Endogenous antigen tunes the
677 responsiveness of naive B cells but not T cells. *Nature* **489**, 160–164 (2012).

678 36. Turner, J. S., Marthi, M., Benet, Z. L. & Grigorova, I. Transiently antigen-primed B cells
679 return to naive-like state in absence of T-cell help. *Nat. Commun.* **8**, 15072 (2017).

680 37. Mesin, L., Ersching, J. & Victora, G. D. Germinal Center B Cell Dynamics. *Immunity*
681 **45**, 471–482 (2016).

682 38. Silver, J. *et al.* Stochasticity enables BCR-independent germinal center initiation and
683 antibody affinity maturation. *J. Exp. Med.* **215**, 77–90 (2018).

684 39. O'Keefe, T. L., Williams, G. T., Batista, F. D. & Neuberger, M. S. Deficiency in CD22, a
685 B cell-specific inhibitory receptor, Is sufficient to predispose to development of high
686 affinity autoantibodies. *J. Exp. Med.* **189**, 1307–1313 (1999).

687 40. Nitschke, L. CD22 and Siglec-G regulate inhibition of B-cell signaling by sialic acid
688 ligand binding and control B-cell tolerance. *Glycobiology* **24**, 807–817 (2014).

689 41. Jellusova, J. *et al.* CD22 × Siglec-G Double-Deficient Mice Have Massively Increased
690 B1 Cell Numbers and Develop Systemic Autoimmunity. (2010).
691 doi:10.4049/jimmunol.0902711

692 42. Hoffmann, A. *et al.* Siglec-G is a B1 cell-inhibitory receptor that controls expansion and
693 calcium signaling of the B1 cell population. *Nat. Immunol.* **8**, 695–704 (2007).

694 43. Bouchon, A., Krammer, P. H. & Walczak, H. Critical role for mitochondria in B cell
695 receptor-mediated apoptosis. *Eur. J. Immunol.* (2000). doi:10.1002/1521-
696 4141(200001)30:1<69::AID-IMMU69>3.0.CO;2-#

697 44. Niiro, H. & Clark, E. A. Regulation of B-cell fate by antigen-receptor signals. *Nat. Rev.*
698 *Immunol.* **2**, 945–56 (2002).

699 45. Dolmetsch, R. E., Lewis, R. S., Goodnow, C. C. & Healy, J. I. Differential activation of
700 transcription factors induced by Ca2+ response amplitude and duration. *Nature* **386**,
701 855–858 (1997).

702 46. Healy, J. I. *et al.* Activated by the B cell receptor during positive versus negative
703 signaling. *Immunity* **6**, 419–428 (1997).

704 47. Haberman, A. M., Gonzalez, D. G., Wong, P., Zhang, T. & Kerfoot, S. M. Germinal
705 center B cell initiation, GC maturation, and the coevolution of its stromal cell niches.
706 *Immunol. Rev.* **288**, 10–27 (2019).

707 48. Akkaya, M. *et al.* Second signals rescue B cells from activation-induced mitochondrial
708 dysfunction and death. *Nat. Immunol.* **19**, 871–884 (2018).

709 49. Siffrin, V. *et al.* FRET based ratiometric Ca^{2+} imaging to investigate immune-mediated
710 neuronal and axonal damage processes in experimental autoimmune
711 encephalomyelitis. *J. Neurosci. Methods* **249**, 8–15 (2015).

712 50. Radbruch, H. *et al.* Intravital FRET: Probing cellular and tissue function in Vivo. *Int. J.*
713 *Mol. Sci. Int. J. Mol. Sci* **16**, 11713–11727 (2015).

714 51. Mayer, C. T. *et al.* The microanatomic segregation of selection by apoptosis in the
715 germinal center. *Science (80-.).* **358**, eaao2602 (2017).

716 52. Pone, E. J. *et al.* Toll-Like Receptors and B-Cell Receptors Synergize to Induce
717 Immunoglobulin Class-Switch DNA Recombination: Relevance to Microbial Antibody
718 Responses. *Crit. Rev. Immunol.* **30**, 1–29 (2010).

719 53. Pone, E. J. *et al.* BCR-signalling synergizes with TLR-signalling for induction of AID
720 and immunoglobulin class-switching through the non-canonical NF-κB pathway. *Nat.*
721 *Commun.* **3**, 712–767 (2012).

722 54. Eckl-Dorna, J. & Batista, F. D. BCR-mediated uptake of antigen linked to TLR9 ligand

723 stimulates B-cell proliferation and antigen-specific plasma cell formation. *Blood* **113**,
724 3969–3977 (2009).

725 55. Ruprecht, C. R. & Lanzavecchia, A. Toll-like receptor stimulation as a third signal
726 required for activation of human naive B cells. *Eur. J. Immunol.* **36**, 810–816 (2006).

727 56. Nguyen, Y. H., Lee, K. Y., Kim, T. J., Kim, S. J. & Kang, T. M. CD40 co-stimulation
728 inhibits sustained BCR-induced Ca2+signaling in response to long-term antigenic
729 stimulation of immature B cells. *Korean J. Physiol. Pharmacol.* **15**, 179–187 (2011).

730 57. Sörman, A., Zhang, L., Ding, Z. & Heyman, B. How antibodies use complement to
731 regulate antibody responses. *Mol. Immunol.* **61**, 79–88 (2014).

732 58. Garside, P. Visualization of specific B and T lymphocyte interactions in the lymph
733 node. *Science (80-.).* **281**, 96–99 (1998).

734 59. Allen, C. D. C., Okada, T. & Cyster, J. G. Germinal Center Organization and Cellular
735 Dynamics. **27**, 190–202 (2008).

736 60. Liu, D. *et al.* T-B-cell entanglement and ICOSL-driven feed-forward regulation of
737 germinal centre reaction. *Nature* **517**, 214–218 (2015).

738 61. Phan, T. G., Green, J. A., Gray, E., Xu, Y. & Cyster, J. G. Immune complex relay by
739 subcapsular sinus macrophages and noncognate B cells drives antibody affinity
740 maturation. *Nat. Immunol.* **10**, 786–796 (2009).

741 62. Weisel, F. J., Zuccarino-Catania, G. V., Chikina, M. & Shlomchik, M. J. A Temporal
742 Switch in the Germinal Center Determines Differential Output of Memory B and
743 Plasma Cells. *Immunity* **44**, 116–130 (2016).

744 63. Kass, G. E. N. & Orrenius, S. Calcium signaling and cytotoxicity. *Environ. Health*
745 *Perspect.* **107**, 25–35 (1999).

746 64. Shanmugapriya, K., Kim, H. & Kang, H. W. In vitro antitumor potential of astaxanthin
747 nanoemulsion against cancer cells via mitochondrial mediated apoptosis. *Int. J.*
748 *Pharm.* **560**, 334–346 (2019).

749 65. Jang, H. D., Hwang, H. Z., Kim, H. S. & Lee, S. Y. C-Cbl negatively regulates TRAF6-
750 mediated NF-κB activation by promoting K48-linked polyubiquitination of TRAF6. *Cell.*
751 *Mol. Biol. Lett.* **24**, 1–13 (2019).

752 66. Mank, M. *et al.* A genetically encoded calcium indicator for chronic in vivo two-photon
753 imaging. *Nat. Methods* **5**, 805–811 (2008).

754 67. Rakhymzhan, A. *et al.* Synergistic Strategy for Multicolor Two-photon Microscopy:
755 Application to the Analysis of Germinal Center Reactions in Vivo. *Sci. Rep.* **7**, (2017).

756 68. Leben, R., Köhler, M., Radbruch, H., Hauser, A. E. & Niesner, R. A. Systematic
757 enzyme mapping of cellular metabolism by phasor-analyzed label-free NAD(P)H
758 fluorescence lifetime imaging. *Int. J. Mol. Sci.* **20**, 1–19 (2019).

759 **Acknowledgements**

760 We thank Patrick Thiemann, Vivien Theissig and Manuela Ohde for animal caretaking. We
761 thank Robert Günther for excellent surgical assistance and Peggy Mex for cell isolations and
762 stainings. We thank Ralf Uecker for microscope facility services. Further thank goes to
763 Mathis Richter for his help with SNR exclusion analysis and proofreading of the manuscript.
764 This study has been supported by the DFG grant TRR130.

765 **Author contributions**

766 A.E.H, R.A.N. and C.U. designed the study and single experiments. F.K. kindly provided
767 mice. C.U. and A.R. conducted experiments. R.L., A.R. and R.A.N. developed mathematical
768 analysis strategies and provided bioinformatical support. L.N. supported with expertise in
769 flow cytometric calcium flux measurements. H.R. provided help for general approach of
770 GECI experiments. C.U., R.L., A.E.H. and R.A.N wrote the manuscript.

771 **Additional information**

772 Supplementary information is available for this paper.

773 Competing interest: The authors declare no competing financial interests.

774 Correspondence: All requests for additional information and material should be addressed to
775 hauser@drfz.de.

776 Reprints and permission information is available online at:

777 A preprint of this paper is available at bioRxiv: https://doi.org/10.1101/2019.12.13.872820